Investigation of Thermal-Induced Strains in Flexible Pavements

Authors:

Mohammad Hossein Shafiee, MSc

Graduate student, University of Alberta

Simita Biswas, BSc

Graduate student, University of Alberta

Negar Tavaf Zadeh, MSc

Graduate student, University of Alberta

Leila Hashemian, PhD

Postdoctoral fellow, University of Alberta

Alireza Bayat, PhD, PEng (Corresponding Author)

Assistant Professor, University of Alberta

(email) abayat@ualberta.ca

Address:

Markin/CNRL Natural Resources Engineering Facility

9105 116th St.

Edmonton, AB Canada T6G 2W2

Paper prepared for presentation at the

Climate Change Considerations for Geotechnical and Pavement Materials Engineering Session

of the 2015 Conference of the Transportation Association of Canada

Charlottetown, PEI

ABSTRACT

Thermal fatigue cracking occurs when the daily temperature cycles cause reoccurring tensile stress at the bottom of the Hot Mixed Asphalt (HMA) layer. Hence, daily temperature variations are considered to be a direct impact of environmental factors on flexible pavements. These stresses may not exceed the tensile strength of the asphalt but, when repeated over time, cyclic loading will cause occurrence of thermal cracks. Therefore, it is necessary to experimentally quantify the range of variation for thermal-induced strains in order to evaluate the impact of daily and seasonal temperature fluctuations on the thermal fatigue cracking.

This paper attempts to investigate the thermal-induced strains in longitudinal, transverse, and vertical directions at the bottom of the HMA over the course of a one year monitoring period. This study was conducted at the Integrated Road Research Facility (IRRF)'s test road in Edmonton, Alberta, Canada, which is fully-equipped with structural and environmental monitoring instruments. Based on the results, noticeable variations for horizontal and vertical strains at the bottom of the HMA were found, especially during the thaw season. Additionally, a consistent relationship is established between thermal-induced transverse and horizontal strains.

Keywords: thermal-induced strains, thermal fatigue cracking, asphalt strain gauge, seasonal variation

INTRODUCTION

Thermal cracking of asphalt concrete pavements can be categorized as low-temperature and thermal-fatigue cracking. While low-temperature cracks occur when the tensile thermal stresses exceed the tensile strength of the HMA, cyclic diurnal temperature fluctuations can cause thermal fatigue cracking (Doré and Zubeck, 2009). In other words, temperature fluctuations can induce repetitive variation of thermal strains in the HMA layer which leads to the occurrence of pavement cracks in the long term (Huang, 1993). It is well documented in the literature that thermal-induced strains at the bottom of the HMA can be reasonably comparable to the strains caused by traffic despite the lower frequency of thermal loading in contrast to that of traffic loading (Bayat *et al.* 2012; Tarefder and Islam, 2013a). Therefore, it is vital to quantify the asphalt strain amplitude associated with thermal loading on flexible pavements due to its critical role in pavement performance. Focusing on horizontal strains at the bottom of the HMA, studies have been performed to evaluate the corresponding variation in thermal-induced strain through field experiments (Bayat *et al.* 2012; Tarefder and Islam, 2013b and Al-Qadi *et al.* 2005). Al-Qadi *et al.* (2005) recorded and analyzed longitudinal strains at the bottom of the HMA layer at the Virginia Smart Road test facility in Montgomery County, Virginia, using Asphalt Strain Gauges (ASGs) over the course of one year. Defining the cyclic strain range as the difference between maximum and minimum strain in a diurnal temperature cycle, longitudinal strain range as high as 350 μm/m was found in mid-April 2014. Results of another experimental program, conducted at the Center for Pavement and Transportation Technology (CPATT) test track in Waterloo, Ontario, Canada, also showed that the highest longitudinal strain range equal to 680 μm/m occurred in mid-May, 2004 (Bayat, 2009). In a recent study, Islam and Tarefder (2014) studied the variations of transverse and longitudinal strains at different depths within HMA at a test road on I-40 interstate highway in New Mexico, United States. The study revealed that anisotropic properties of the HMA against thermal loading can be significant in different seasons.

The reviewed studies demonstrate that investigation and quantification of thermal-induced strains play a significant role in evaluation of flexible pavement performance in terms of thermal fatigue cracking. While previous studies have mostly focused on the horizontal strain, i.e. in longitudinal and transverse directions at the bottom of the HMA, there is a need to comprehensively analyze both horizontal and vertical cyclic strain fluctuations as a result of temperature changes.

In this paper, findings from an experimental program carried out at the Integrated Road Research Facility (IRRF) located in Edmonton, Alberta, Canada, were used to study the thermal-induced HMA strains from October 2013 to October 2014. By examining the seasonal changes of thermal strains in three directions versus the ambient air temperature data, this paper will also focus on the magnitude of irrecoverable strains at the end of the monitoring period.

EXPERIMENTAL PROGRAM

SITE INFORMATION

The newly constructed IRRF test road facility will function as an access road to Edmonton Waste Management Center (EWMC). It is tentatively scheduled to open to traffic in the summer

of 2015. As shown in Figure 1, the flexible pavement structure consists of the two types of HMA layers as wearing and binder courses placed on top of granular base course (GBC) on a clayey sand (SC) subgrade. Table 1 illustrates the fundamental physical properties of the binder and wearing layers which were laid in August 2012 and October 2013, respectively. Reclaimed Asphalt Pavement (RAP) with the average recovered asphalt cement content of 5.0 percent by mass of dry aggregate was used in both HMA mixtures. Besides, the virgin asphalt cement classified as PG 58-28 was incorporated in both mixtures. The wearing mix possessed a maximum aggregate size of 12.5 mm, while the maximum aggregate size was 25 mm for the binder mix.

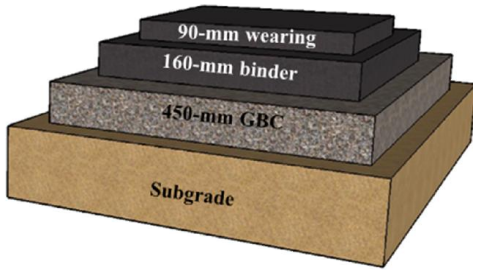

FIGURE 1 Pavement cross section at the IRRF.

TABLE 1 Physical properties of wearing and binder layers.

Property	Asphalt Physical Properties	
	Wearing	Binder
Max. Aggregate size (mm)	12.5	25.0
Virgin Binder Grade	PG 58-28	PG 58-28
RAP Binder Grade	PG 70-28	PG 70-28
Blended Binder Grade	PG 58-28	PG 58-28
Percentage of incorporated RAP (%)	20.0	10.0
Binder Content by Weight of Mix (%)	4.6	5.3
Void in Mineral Aggregate (VMA) (%)	13.1	14.3
Void Filled with Asphalt (VFA) (%)	69.4	74.9
Air Voids (%)	4.0	3.6
Density (kg/m3)	2355	2344
Marshal Stability (KN)	17.7	16.9
Flow (mm)	2.3	2.5
Theoretical Film Thickness (μm)	6.7	7.1
Tensile Strength Ratio (TSR) (%)	98.0	81.6

According to the Unified Soil Classification System (USCS), the subgrade soil was classified as Clayey Sand (SC) having a maximum particle size of 0.5 mm, liquid limit of 25 and plastic index of 9 percent. The GBC, composed of crushed aggregates with a maximum size of 19 mm, was classified as Well-Graded Gravel (GW) according to the USCS standards. Figure 2 depicts the schematic plan view of the IRRF's test road in which two pavement monitoring sections are designed to capture the structural and environmental response of different layers. These two sections were instrumented in a similar manner during the road's construction in the summer of 2012. The collected data is retrieved from the data center at the IRRF using a remote monitoring system which decreases the number of unnecessary site visits.

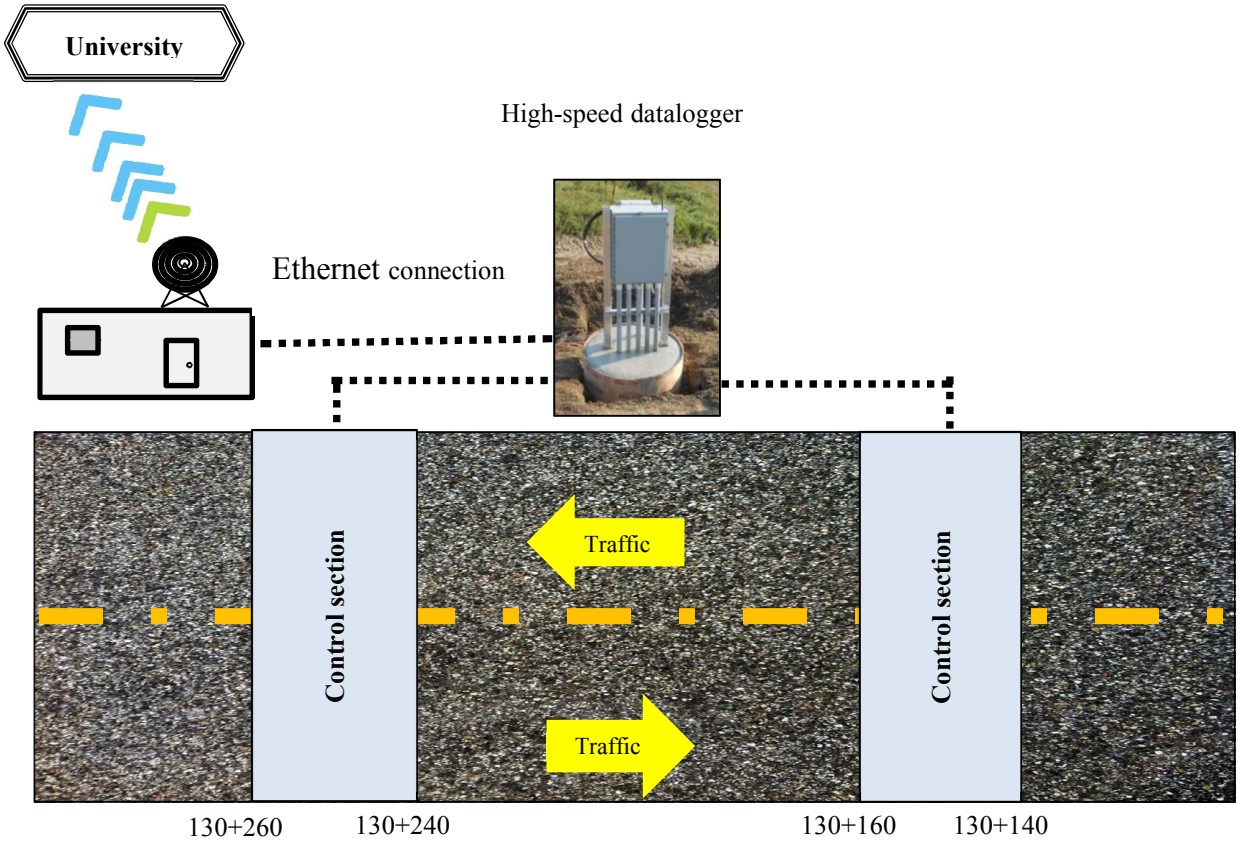

FIGURE 2 Pavement monitoring sections at IRRF's test road.

INSTRUMENTED SECTIONS

A total of eighteen ASGs including six in the longitudinal direction (ASG-L), six in the transverse direction (ASG-T), and six in the vertical direction (ASG-V) were installed at 250-mm depth in the HMA layer in each section. In addition, other gauges such as Earth Pressure Cells (EPC), Time Domain Reflectometrs (TDR) and asphalt thermistors were placed within the

structure for comprehensive data collection at the IRRF. Figure 3 shows the cross section of the pavement monitoring control sections in parallel with the traffic direction. Strain and stress data are collected via a CR9000X datalogger at 15-min intervals in static mode and 0.002-s intervals in dynamic mode. Similarly, both temperature and moisture data are recorded at 15-min intervals using a CR1000 datalogger.

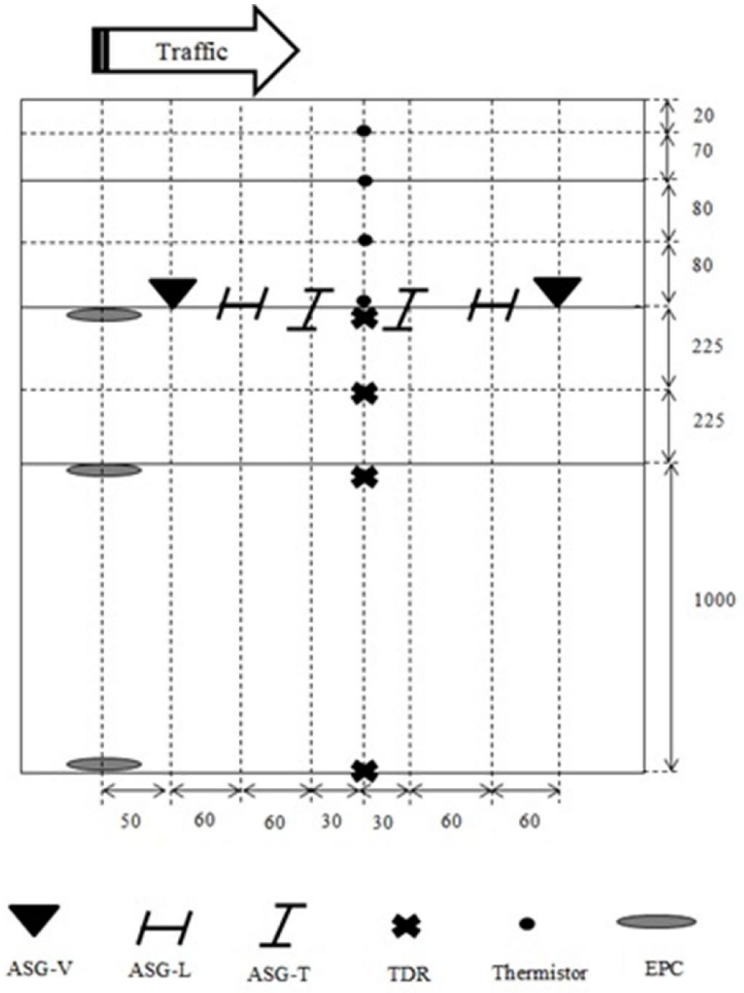

FIGURE 3 Plan view of the test sections at the IRRF (All units in mm).

As shown in Figure 4, the layout of the ASG(s) was designed to capture the responses along the outer wheel path (line B) as well as two additional offsets of 600 mm to the left (line A) and 600 mm to the right (line C). In this study, static strain data from three ASGs in section 1 and located along line B were utilized as similar trends were observed in all three groups of the gauges. Moreover, ambient air temperature data was obtained from the closest weather station at the EWMC, which was located about 700 m north of the test road. Over the course of October 2013 to October 2014, the maximum and minimum average hourly ambient air temperatures were equal to 38.5˚C and -30.0˚C, respectively.

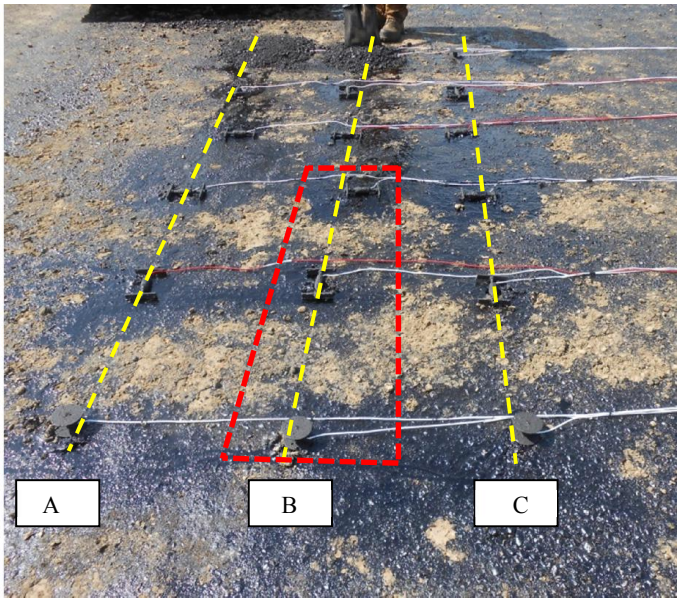

FIGURE 4 Instrumentation array at three offsets (lines A, B and C) at the bottom of the HMA.

THERMAL LOADING CYCLE

In order to investigate the development of thermal strain at the bottom of HMA, variations of the three types of strain as well as temperature are typically plotted in Figure 5. Plotting longitudinal strain (ε_l), transverse strain (ε_t) and vertical strain (ε_v) data collected on September 17, 2014, clearly shows the identical trends between ambient air temperature and induced strains. It is evident from Figure 5 that as the temperature decreases, thermal contraction becomes more notable for all strains. However, with the temperature increase from the late morning until 6:00 PM, thermal expansion was observed in the three directions in the HMA layer. While the pavement surface is exposed to high ambient air temperature and significant solar radiation during the day, the heat will be gradually transferred to the bottom of the HMA, leading to its expansion. Reversely, the stored heat starts to dissipate from the top overnight which can in turn trigger the contraction of the HMA. From the observed cyclic behavior of the thermal-induced strains, it can be inferred that the frequency of thermal loading was equal to one day. This agrees with the findings in the previously discussed studies which reported one cycle of thermal loading per day for longitudinal strain gauges (Bayat *et al.* 2012; Tarefder and Islam, 2013b and Al-Qadi *et al.* 2005). It was found that the peak-to-peak magnitude of ε_l was near 200 μm/m which was larger than that of ε_t (90 μm/m) and ε_v (150μm/m). The observed strain fluctuations corresponded to 20°C change in ambient air temperature. It is worth noting that the induced thermal strains lagged the temperature variation by almost four hours partially due to the relatively high thickness of the HMA which hinders the heat penetration and dissipation.

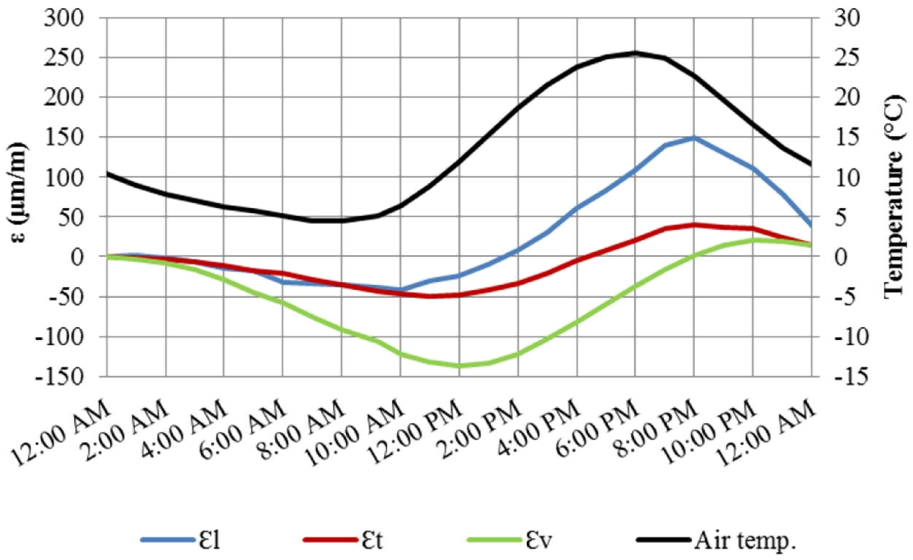

FIGURE 5 Thermal loading cycles and temperature readings on September 17, 2014

SEASONAL MONITORING OF THERMAL INDUCED STRAIN

Figures 6 to 8 illustrate the seasonal variation of in-situ measured ε_l, ε_t and ε_v, respectively, during the one-year monitoring period from October, 2013 until October, 2014. All measured strain data were zeroed against the associated values recorded on October 1, 2013. Small gaps in data measurements exist from February 27, 2014 to March 14, 2014 for ε_l and ε_t and from April 28, 2014 to May 13, 2014 for ε_v because of a technical issue in the data collection system.

Figure 6 depicts the measured ε_l by ASG-L2 and ambient air temperature in which similar trends were noted between strain and temperature. The minimum and maximum magnitudes of ε_l were determined equal to 789 μm/m and – 556 μm/m recorded on July 29, 2014 and February 10, 2014, respectively. The associated average daily temperatures were 21°C on July 29, 2014 and -21°C on February 10, 2014, as well. The obtained results showed that the average ε_l during the fall (October to December, 2013) was around 50 μm/m, while that value decreased to -92 μm/m in the winter (January, 2014 to March, 2014), and later increased to 170 μm/m in the spring (April to June, 2014). Consequently, the average ε_l values were found equal to 459 and 285 μm/m during the summer (July to September, 2014). According to Figure 6, the recorded ε_l did not return to its initial value at the end of monitoring period implying accumulation of irrecoverable strain at the bottom of the HMA.

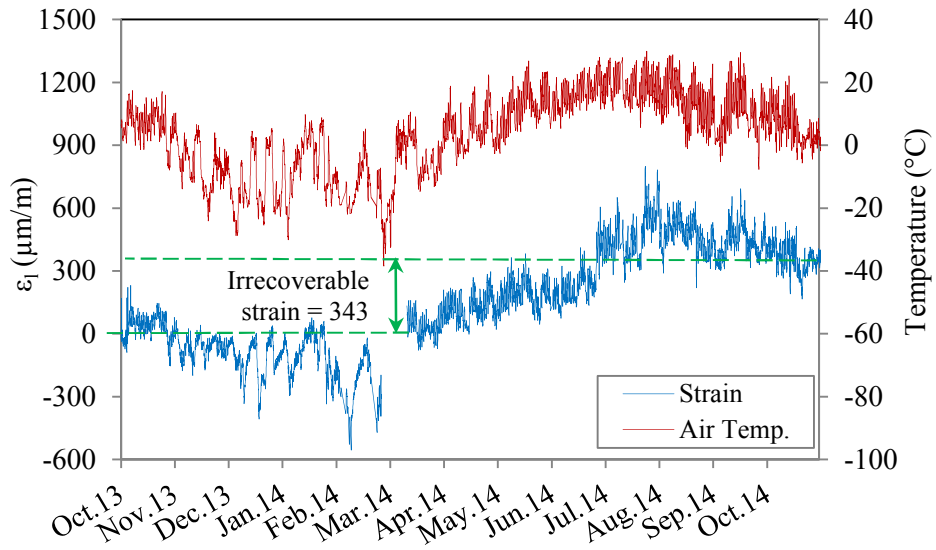

FIGURE 6 Variation of ε_l from October, 2013 to October, 2014.

Similarly, the variation of ε_t measured by ASG-T2 is depicted in Figure 7 in which strain followed the same pattern as temperature. The average ε_t in each season was determined to be -29 μm/m in the fall, -33 μm/m in the winter, 154 μm/m in the spring and 260 μm/m in the summer. The maximum and minimum ε_t of 444 μm/m and - 344 μm/m were obtained on July 29, 2014 and February 10, 2014 when the average daily temperature was 21°C and - 21°C, respectively. It should be noted that ε_t was generally lower than ε_l. Besides, the magnitude of irrecoverable ε_t at the end of the monitoring period was found lower than that of ε_l.

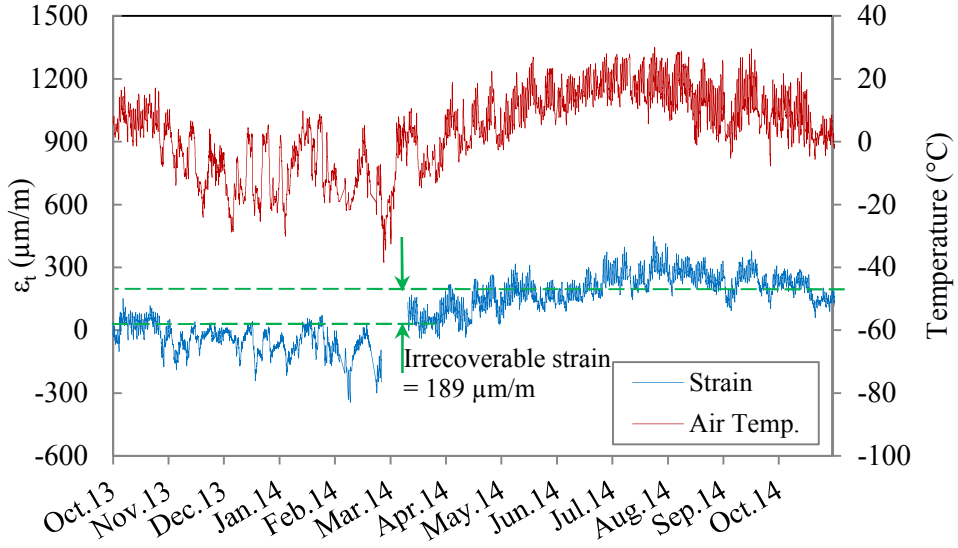

FIGURE 7 Variation of ε_t from October, 2013 to October, 2014.

Data from ASG-V2 was used to plot the variation of ε_v as shown in Figure 8. During the monitoring period, temperature fluctuations clearly affected the ε_v at the bottom of the HMA. According to Figure 8, on September 22, 2014, with the average temperature of 19°C, the highest ε_v of 1403 µm/m was attained. In contrast, the minimum ε_v was recorded as -336 µm/m on March 29, 2014 with the average temperature of -3°C. Considering the seasonal average of ε_v over a one-year analysis period, the average ε_v in the fall, winter, spring, summer was determined equal to -70, -116, 153 and 965 µm/m, respectively. The magnitude of irrecoverable ε_v was found significantly larger than those of horizontal strains. Based on Figures 6 to 8, it was observed that ε_v experienced the highest fluctuations in comparison to horizontal strains.

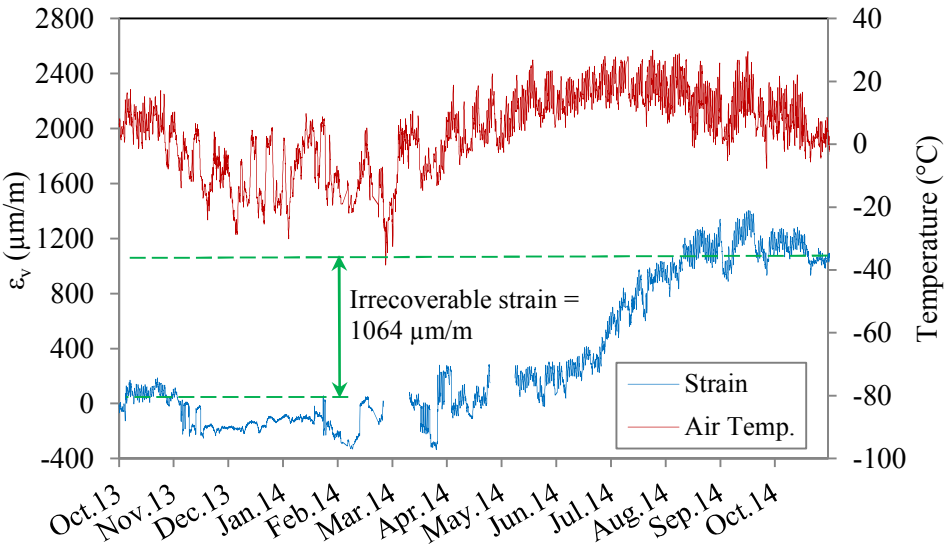

FIGURE 8 Variation of ε_v from October, 2013 to October, 2014.

Figure 9 compares the monthly average strains as well as the ambient air temperature. According to Figure 9, the obtained values generally increased at higher temperatures; nonetheless, the accumulation of irrecoverable strain was observed in the colder months. It was also found that the highest horizontal strains captured in August 2014 did not coincide with the highest vertical strain obtained in September 2014. Based on Figure 9, the monthly average ε_v remained higher than horizontal strains since June 2014.

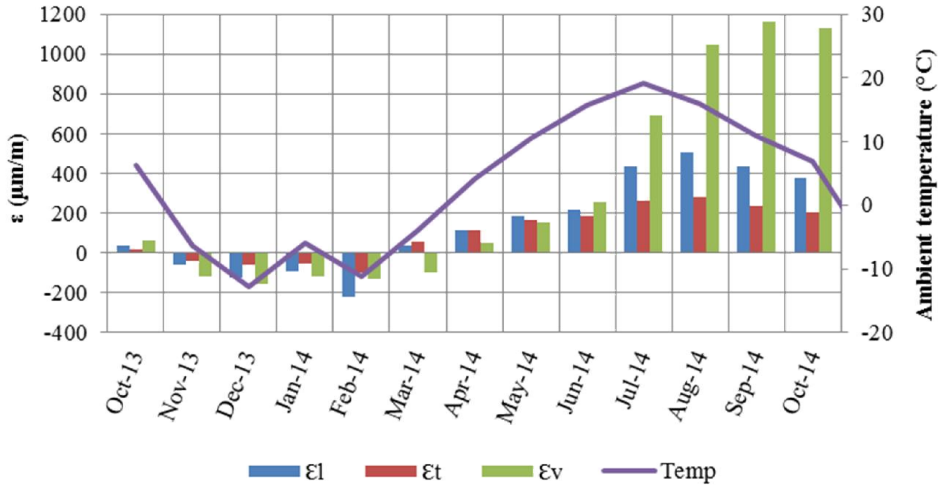

FIGURE 9 Monthly average strains from October, 2013 to October, 2014.

Since the criticality of cyclic temperature fluctuation in development of thermal-induced strains can be determined based on the calculation of cyclic strain range rather than peak strain values (Al-Qadi *et al.* 2005), strain results were processed to find the cyclic strain ranges. By calculating the difference between maximum and minimum strains in each cycle ($\Delta\varepsilon$), strain ranges were found for each day using Equation 1

$$\Delta\varepsilon = \varepsilon_{max} - \varepsilon_{min} \quad (1)$$

where $\Delta\varepsilon$ is the daily thermal-induced strain range, ε_{max} is the maximum daily strain and ε_{min} is the minimum daily strain.

Later, the monthly average strain ranges were computed as shown in Table 2. Results showed that the strain range in longitudinal direction ($\Delta\varepsilon_l$) was distinctly larger than those in transverse ($\Delta\varepsilon_t$) and vertical ($\Delta\varepsilon_v$) directions. According to Table 2, $\Delta\varepsilon_l$ and $\Delta\varepsilon_t$ reached their maximum in July and April 2014, respectively; however, maximum ε_l and ε_t occurred in August 2014. Moreover, maximum $\Delta\varepsilon_v$ and ε_v were detected in September 2015. In addition, the observed strain ranges typically tended to increase during the warmer months of the year.

TABLE 2 Monthly average thermal-induced strain range

Month	$\Delta\varepsilon_l$ (μm/m)	$\Delta\varepsilon_t$ (μm/m)	$\Delta\varepsilon_v$ (μm/m)
October-13	111	95	88
November-13	83	63	32
December-13	100	58	24
January-14	106	78	56
February-14	107	88	65
March-14	123	105	139
April-14	142	121	134
May-14	149	108	136
June-14	131	82	137
July-14	192	116	157
August-14	163	97	162
September-14	144	91	178
October-14	147	72	124

RELATIONSHIP BETWEEN HORIZONTAL STRAIN RANGES

To investigate the relationship between horizontal strain ranges at the bottom of the HMA, the daily fluctuation of $\Delta\varepsilon_l$ and $\Delta\varepsilon_t$ were plotted against each other as depicted in Figure 10. Fitting a linear regression line, using least squared method to correlate two parameters, a predictive equation was derived. The established regression correlation suggests a good relationship between two parameters with an R^2 value of 0.8, standard error of estimate (S_e) equal to 15.10 and standard deviation (S_y) as 34.05. According to the criteria indicated in the literature (McCuen, 2002), the regression equation is worthwhile as the value of S_e is noticeably smaller than S_y. The S_e/S_y ratio of 0.44 indicates that the regression correlation significantly improves the accuracy of prediction. The developed correlation shows that $\Delta\varepsilon_l$ was generally larger than $\Delta\varepsilon_t$ during the monitoring period. The larger $\Delta\varepsilon_l$ values confirm that strains in longitudinal direction can be responsible for initiation of transverse cracks due to thermal fatigue cracking as also reported by Al-Qadi *et al*. (2005).

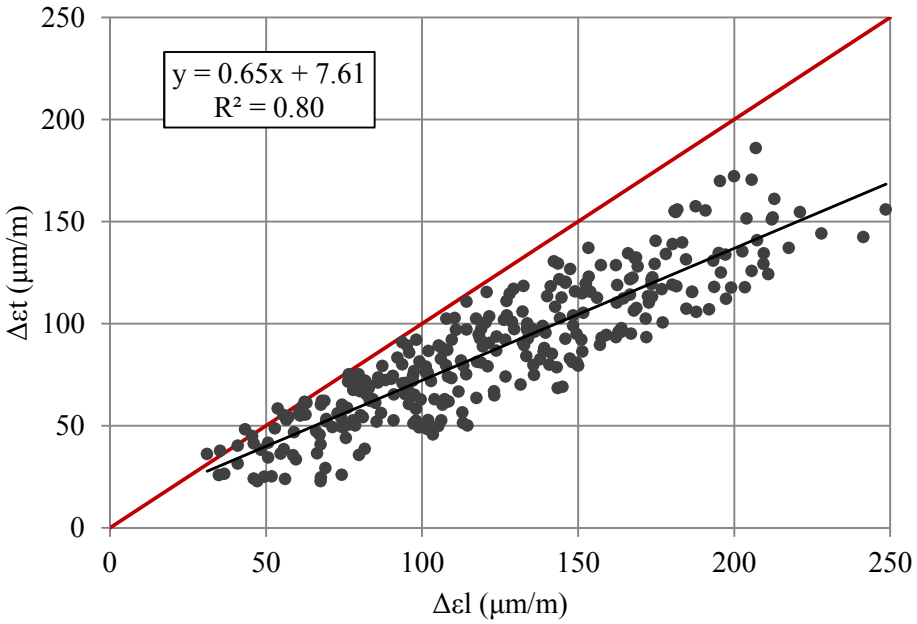

FIGURE 10 Comparison of $\Delta\varepsilon_t$ against $\Delta\varepsilon_l$ at the bottom of the HMA.

CONCLUSION

Field measurements for ε_l, ε_t, and ε_v were conducted at the IRRF's test road to monitor the impact of daily fluctuation and seasonal change in ambient temperature on the developed responses at the bottom of the HMA. Results showed that a similar trend was observed between the fluctuation of the ambient air temperature and the induced strain ranges. In addition, winter and spring were the most critical periods in terms of the highest absolute value for horizontal and vertical strains, while maximum fluctuation of ε_v occurred during the spring-thaw season. This study showed that the maximum strain range was equal to 192 μm/m for ε_l, 116 μm/m for ε_t and 178 μm/m for ε_v. Finally, the irrecoverable ε_v was as high as 3.1 times larger than that of ε_l and 5.6 times larger than the corresponding ε_t value, at the end of a one-year monitoring period. A consistent linear relationship was also established between $\Delta\varepsilon_l$ and $\Delta\varepsilon_t$ daily fluctuations, implying that $\Delta\varepsilon_t$ was approximately 66 percent of $\Delta\varepsilon_l$. In summary, the likelihood of thermal fatigue cracking occurrence is a function of daily and seasonal variation of thermal induced strains. Besides, considering the remarkable impact of temperature on the development of strains at the bottom of the HMA, discretion should be exercised when taking the combined impact of traffic and temperature-induced strains into account for design and performance analysis. Hence, depending on the daily and seasonal variation of the thermal-induced strains, the magnitude of total strains under live traffic can vary. Further research is required to study the extent to which asphalt strain is affected by the combined impact of thermal strain and traffic loading.

ACKNOWLEDGEMENTS

The authors would like to acknowledge Alberta Transportation, Alberta recycling, and The City of Edmonton for providing financial and in-kind support for the construction and instrumentation of the IRRF's test road.

REFERENCES

Al-Qadi, I. L., Hassan, M. M., and Elseifi, M. A. 2005. "Field and Theoretical Evaluation of Thermal Fatigue Cracking in Flexible Pavements." In Transportation Research Record: *Journal of the Transportation Research Board*, No. 1919(1), Transportation Research Board of the National Academies, Washington, D.C., pp. 87-95.

Bayat, A. 2009. "*Field and Numerical Investigation to Determine the Impact of Environmental and Wheel Loads on Flexible Pavement."* Doctoral dissertation, University of Waterloo, Ontario, Canada.

Bayat, A., Knight, M. A., and Soleymani, H. R. 2012. "Field Monitoring and Comparison of Thermal- and Load-induced Strains in Asphalt Pavement." *International Journal of Pavement Engineering*, 13(6), pp.508-514.

Doré, G., and Zubeck, H. K. 2009. "*Cold Regions Pavement Engineering*." American Society of Civil Engineers, Virginia, United States.

Huang, Y. H. 1993. "*Pavement Analysis and Design*." 2nd Edition, Prentice Hall, Inc., Upper Saddle River, New Jersey, United States.

Islam, M. R., and Tarefder, R. A. 2014. "Determining Thermal Properties of Asphalt Concrete Using Field Data and Laboratory Testing." *Construction and Building Materials*, 2014.

McCuen, R. H. 2002. "*Modeling Hydrologic Change: Statistical Methods*." CRC press.

Tarefder, R. A. and Islam, M. R. 2013a. "Measuring Fatigue Damages from an Instrumented Pavement Section due to Day-Night and Yearly Temperature Rise and Fall in Desert Land of the West." In *Climatic Effects on Pavement and Geotechnical Infrastructure*, Proceedings of the International Symposium of Climatic Effects on Pavement and Geotechnical Infrastructure, August 4-7, Fairbanks, Alaska.

Tarefder, R. A. and Islam, M. R. 2013b. "Measuring Thermal Effect in the Structural Response of Flexible Pavement Based on Field Instrumentation." *International Journal of Pavement Research and Technology*, 6(4), pp. 274-279.